Supporting Information

# Tailoring Patches on Particles: A Modified Micro-contact Printing Routine Using Polymer-functionalized Stamps

[a] *Fraunhofer Institute for Applied Polymer Research IAP, D-14476 Potsdam-Golm, Germany.*
[b] *Chair of Polymer Materials and Polymer Technologies, University Potsdam, D-14476 Potsdam-Golm, Germany.*
‡ Both authors contributed equally to this work.
Electronic Supplementary Information (ESI) available: [details of any supplementary information available should be included here].
See DOI: 10.1039/x0xx00000x

Marcel Sperling, ‡[ab] Martin Reifarth, ‡[ab] Richard Grobe[ab] and Alexander Böker*[ab]

## Experimental section

**Materials and instruments:**

Unless stated otherwise, all chemicals were used as received. The silica particles used for the experiments were purchased from Cospheric LLC and possessed the following parameters: 4.08 µm nominal diameters, 1.8 $g \cdot mL^{-1}$ solid density. Rhodamine B isothiocyanate (mixed isomers) as well as (3-aminopropyl) triethoxysilane (APTES, ≥98 %), aqueous ammonia solution (28-30 % w/w) were purchased by Sigma Aldrich. PDMS was prepared on the basis of a commercially available standard kit (SYLGARD® 184, Dow Corning). The polymers used for PDMS modification, *i.e.* methoxy terminated poly(ethylene glycol) triethoxysilane (mPEG-5K-silane) or poly(N-isopropylamino acrylamide) triethoxysilane (PNIPAAm), were obtained from Sigma-Aldrich. Trimethyl chlorosilane (≥99 %), used for glass hydrophobization, was purchased from Sigma-Aldrich as well. All solvents were used as purchased.

Image acquisition was performed using a *Leica DMI-8* fluorescence microscope with proper filter settings to obtain transmission light (TL) and fluorescent light (FL) images. For plasma treatment, a PlasmaFlecto 10 oven was used.

MALDI-ToF spectra were acquired with a 337 nm laser Bruker microflex MALDI-ToF mass spectrometer (Bruker, Bremen, Germany) utilising pulsed ion extraction. Thereby, the masses were determined in positive ion reflective mode. For measurements, the sample solutions were applied on a ground steel target using the dried droplet technique. For this purpose, α-cyano-4-hydroxycinnamic acid (CCA, Sigma Aldrich), was used as matrix substance. Sodium trifluoroacetate (Sigma Aldrich) was used as salt. Mass calibration was performed with external calibration.

**Amino-functionalisation of particles:**

In order to enable covalent attachment of rhodamine dye to the particle surface, the particles were amino-functionalised by chemical vapour deposition (CVD) using APTES. For this purpose, typically 200 mg of dry $SiO_2$-particles were first plasma-activated using air plasma at 100 W, 0.2 mbar for 60 s for three times, thereby gently mixing the dried between each plasma step. In the second step, this as-prepared particles were subjected to a chemical CVD procedure at 80 °C for 2 h by enclosing the particles into a 60 mL PFA-chamber (Carl-Roth) along with 200 µL APTES and 200 µL of a 28-30 % (w/w) aqueous ammonia solution as catalyst, each chemical was thereby placed in separate vials. This process was repeated twice with exchange of APTES, catalyst and gentle mixing of the particles. The final $SiO_2$@$NH_2$-particles were stored as a 10 % (w/v) aqueous suspension.

**Preparation and inking of (modified) polydimethylsiloxane (PDMS) stamps for microcontact printing:**

The bare PDMS gel was produced by mixing precursor and curing agent in a ratio of 5:1 using the standard kit. The highly viscous mixture was then poured into a plastic petri dish up to a filling height of approximately 1 mm. Next, the PDMS gel was aged on an even ground for 16-24 h at ambient conditions, whereupon enclosed gas bubbles vanished, and afterwards cured for two hours at 80 °C. The resulting elastomeric gel was washed in acetone (5 mL per g PDMS) five times for 24 h until the weight was reduced by about 4-5 %, indicating loss of free oligomers resulting from the gel formation. The cured and washed gel was punched into cylindrical stamps with a diameter of 1 cm.

For further functionalisation, the as-prepared bare PDMS-stamps were surface-activated by another plasma treatment step using air plasma at 100 W, 0.2 mbar for 60 s. The activated stamps were then covered with a precursor solution containing the respective polymeric silane agent, *i.e.* methoxy terminated poly(ethylene glycol) triethoxysilane (referred to as mPEG) or poly(N-isopropylamino acrylamide) triethoxysilane (PNIPAAm). The aforesaid solutions were thereby prepared by dissolving the referring silane at 1 $mg \cdot mL^{-1}$ in 50 % ethanol:water (volumetric ratio), further containing 1 % (v/v) of acetic acid as catalyst. The immersed stamps were gently shaken inside a closed vessel for 2 h using a rocking device. Finally, the stamps were each washed with ethanol and dried using a soft air stream.

Inking was performed by loading the respective stamps with a defined volume of a buffered RITC (mixed isomers, $\lambda_{em,max}$ = 555 nm) solution (10 $\mu g \cdot mL^{-1}$, carbonate buffer, I = 15 mM NaCl, pH 9.35), soaking them for 40-45 min in a water-saturated atmosphere in the dark to prevent dye bleaching. In this context, different volumina and temperatures were used as discussed in Table S1 depending on the stamp type. Afterwards, the ink solution was removed by a pipette and additional washing in buffer solution (carbonate buffer, 15mM NaCl, pH 9.35) followed by gentle drying the stamps using a soft air stream.

**Table S1**: Amount of ink solution to ensure complete stamp coverage during inking depending on stamp modification

| **Stamp modification** | **$T_{ink}$ [°C]** | **$V_{RITC}$ [µL]** |
|---|---|---|
| bare PDMS | 20-22 | 200 |
| mPEG5K-silane | 20-22 | 150 |
| PNIPAAm-silane | 20-22; 45 | 100 |

***Particle immobilization & microcontact printing***

The data acquired with this method is presented in Figures 2 and 3 and discussed in the respective part of the manuscript.

Since we intended to measure the dimensions of the patches for all experiments, particle immobilisation on a glass support became mandatory. Particle immobilisation was, furthermore, necessary to ensure that the particles did not change their orientation or were removed upon stamp removal throughout the printing process. This was rendered possible by casting a $SiO_2$@$NH_2$-particle monolayer using a shear-induced assembly process[1] on a plasma activated (300 W, 300 s, 0.2 mbar, oxygen) microscopy glass-slide (26 x 76 mm²), followed by an annealing process for about 1 h at 80 °C. Typically, 15-20 µL of a suspension containing 2.5 % (w/v) $SiO_2$@$NH_2$-particles in 50 % (v/v) was dropped on the glass slide (Figure S1a), and the upper glass plate, which was prepared similarly to the bottom one, was moved horizontally at a constant speed of about 0.25 mm·$s^{-1}$ (Figure S1b) using a syringe pump (WorldPrecision instruments).

To obtain patches *via* microcontact printing, the inked stamp was placed onto the monolayer and subjected to pressure by using a specific weight (*i.e.* 50 g or 100 g) for 5-10 s on top of the stamp (Figure S1c) with subsequent stamp removal. Due to the particle immobilisation on the glass substrate, fluorescence microscopy could be performed from printing site using a fluorescence microscope. The resulting transmission light (TL) and fluorescent light (FL) images were acquired such that the sample was scanned at different z-positions from particle layer top to bottom. With that method, we could ensure proper sample focus (Figure S1d). As objective, we employed a 40x dry objective with a numerical aperture of 0.8. The samples were all measured at the same illumination and detector settings.

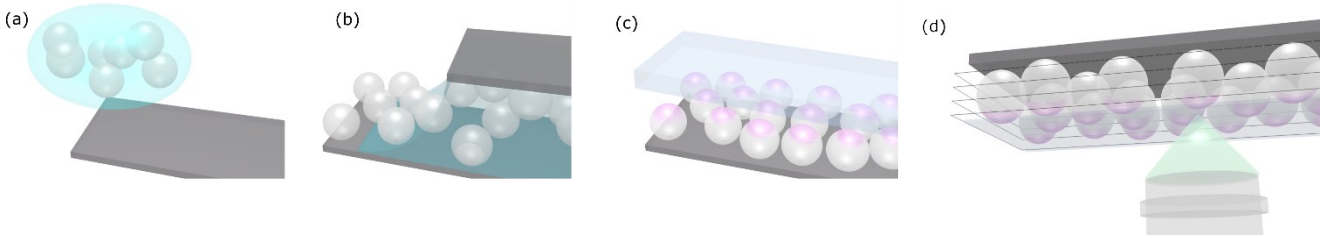


**Figure S1:** Schematic overview over the sample preparation. (a) A small amount of particle suspension was casted on the pre-treated glass substrate. (b) By shearing a second glass plate over the first one, self-assembly of the particles resulted to form well-defined particle monolayers. (c) µCP was performed on the particle monolayer by utilising a (polymer-grafted) PDMS stamp. (d) A high-precision microscopy coverslip was placed on the resulting monolayer of patchy particles to facilitate fluorescence microscopy investigations. Here, the particles are not embedded in any liquid, but kept in air. Microscopy was thereby performed from the printing side. In this context, a z-stack with different focus positions through the particle monolayer was acquired.

### *Remark on the experimental imaging conditions*

It deserves particular mention here that we employed a dry objective with a low numerical aperture (40x/NA 0.8) for our experiments. While being a rather sophisticated NA for a dry objective, the utilisation of an objective with NA = 0.8 supports only a mediocre performance of the microscope as dictated by the *Rayleigh* criterion (0.6 λ / NA) for optical resolution (the lateral xy-resolution of a fluorescence microscope as used here is approx. 430 nm). For improved resolution, objectives with NA values greater than 1.2 must be utilised, and in sight of recent developments in fluorescence microscopy focusing on high-resolution techniques, it might be critically remarked that we do not implement this improved instrumentation in our experiments.

This can be attributed to the fact that high NA microscope objectives are particularly prone to optical aberrations in terms of spherical aberrations, which drastically reduce the image quality. These may occur as a result of refractive index (RI) inhomogeneities within the sample. A reduction of these aberrations can, however, be achieved by embedding the object of investigation (*i.e.* the particles) in a matching RI embedding medium (to match the RIs of the objective immersion medium, and the investigated particles and surrounding space) and applying immersion fluids (*e.g.* water, glycerol, oil) between the objective lens and the coverslip of the sample. During our measurements, however, we strictly omitted embedding the imprinted particles into any liquid, since we intended

to obtain an impression of the printing process. This requires imaging of the particles under strictly dry conditions directly after printing to avoid a diffusive detachment of the ink material from the particle surface potentially occurring in solution. As a consequence of this, the avoidance of any immersion liquids was indicated, since this would provoke a RI mismatch of the sample and objective medium, respectively, which is particularly pronounced when going from a denser objective medium into a less dense sample one.

On the other side, alongside these experimental difficulties, we do not expect that an improved resolution would in our case be a real benefit for the data elaboration. Utilising the aforementioned dry objective, we expect a typical resolution of about 427 nm (considering the $\lambda_{em,max}$ = 560 of Rhodamine 2B). Compared to that, this resolution would be slightly better at 280 nm for a comparable confocal setup. Since the smallest patches observed are at least around 1 µm, both resolutions are suitable enough to elucidate the patch dimensions. Resolution, thereby, is defined as the minimum resolvable distance between two separately identifiable objects. In our images, we worked at a typical scale of 6.2 px·µm$^{-1}$, which means that the pixel-size is about a factor of 2.6 below the aforementioned resolution limit. In other words, about 2.6 pixels correspond to the minimum resolvable distance. Resolvable distance means that the peaks of the point spread functions (PSF) of each pixel are distant enough for their separate detection as distinct individual peaks, *i.e.* two separate objects. Below this limit, two functions will merge towards a single combined one. Since we were not interested in the internal morphology of the patches, rather than the overall intensity profile of the patch area, the merge of PSFs towards a single PSF will still be affected by the intensity differences. Accordingly, our setup still allows for an evaluation of the overall profile, as long as the patch area is well within the detection limit, while a better resolution would result in more distinct data points for the intensity profile functions that are shown in Figure 3. Said intensity profiles in Figure 3 show enough points for a clear shape and reliable fit, whose quality we would deem to be neither enhanced nor altered in a significant way upon increase of the resolution.

***Preparation of dispersed patchy particles***

The data acquired with this method are presented in Figure 4 in the manuscript.

In order to prepare isolated patchy particles the above mentioned monolayer casting procedure was adapted, in that the glass substrate was modified using trimethyl chlorosilane *via* a CVD process after the plasma treatment for hydrophobisation of the glass substrate. In a next step, the $SiO_2$@$NH_2$-particles were dropped in a suspension of 10 % (w/v) in 80 % (v/v) n-propanol in water. The hydrophobisation thereby promotes particle transfer to the stamp during the printing procedure – almost to a complete extent – instead of their immobilisation on the glass substrate.

The particle containing stamp was ultrasonicated (37 kHz, 25 min, RT) in a 5 mL tube using ethanol to liberate the particles. Afterwards, the particles were centrifuged (RCF 8100, 2 min) and washed with ethanol for three times and subsequently dispersed in a small amount of ethanol (20-30 µL). The particles were dropped on a microscopy slide, which was covered by a coverslip. This sample was sealed and further subjected to light microscopy.

## Image evaluation and quantification algorithm

In this section, our developed image evaluation routine is explained by a detailed walkthrough (see also Figure S2 below).

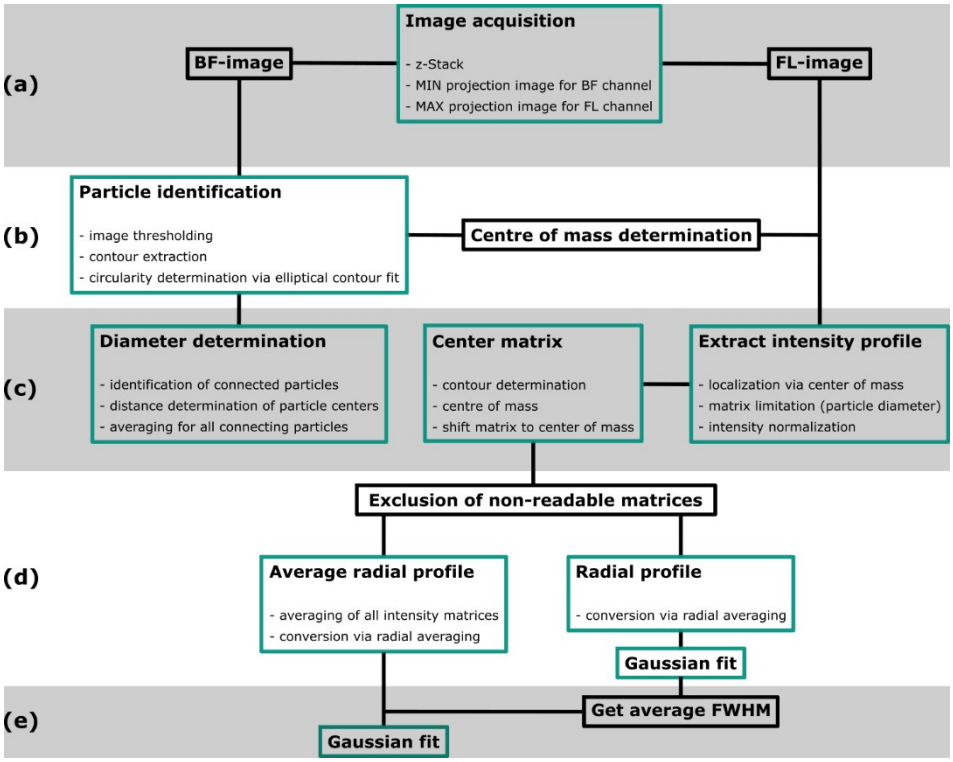


**Figure S2:** Schematic representation of the image processing routine for the determination of the patch intensity profiles: (a) An image sequence consisting of a light transmission and fluorescence widefield channel is acquired as a z-stack. The corresponding stacks are transformed to the minimum projection for the brightfield (BF) and the maximum projection for the fluorescence (FL) channel; (b) particle centres of mass are identified *via* contour extraction and filtered using thresholding and circularity criteria; (c) particle diameters are assessed here *via* the determination of pairwise centre distances. The fluorescence normalized intensity profiles are extracted for each particle and centred; (d) readable profiles are converted to radial profiles individually and as average, wherein individual profiles are each fitted with a Gaussian profile yielding FWHM values (*i.e.* patch diameters); (e) FWHM values are averaged and used as parameter for fitting a Gaussian profile to the average radial profile the average.

In order to ensure proper focus of every particle within the image, z-stacks are acquired and transferred to a projected image with the brightfield (BF) channel as minimum (MIN) and the fluorescence (FL) channel as maximum (MAX) projection using Fiji/ImageJ,[2] see Figure S2 (a).

The projected BF-image (MIN-BF) is then subjected to a thresholding routine and the resulting contours are extracted including their centres of mass using openCV in Python,[3] so that the particles are identified from the image objects, see Figure S2 (b).

The obtained centres of mass, subsequently, serve as anchor coordinates for the extraction of the corresponding fluorescence intensity profile from the correlating FL-image (MAX-FL). More in detail, the fluorescence intensity matrix is extracted from the MAX-FL image by consideration of a known average particle size (~4 µm) and the previously determined particle centre to yield each particle's fluorescence intensity profile. Next, the extracted profile is normalized to its maximum and subjected to a contour extracting routine, analogously to the one mentioned in step (a) above, and the respective centre of mass is then compared with the centre of mass obtained from the BF-MIN image. Calculating the difference of these two points yields a shift vector, which is then used to shift the intensity matrix to the particle centre. This is performed to avoid artificial broadening of the patch profile during averaging over all particle profiles (Figure S2c).

In addition to the determination of the signal intensity from the fluorescence images, the brightfield transmission light microscopy images were subjected to analysis to provide the diameters of the particles. For this purpose, diameters are calculated from the MIN-BF image from at least pairwise closely packed particles using the average distance of their centres of mass, see Figure S2 (c).

On the occurrence of non-readable intensity profiles, *e.g.* centre of mass of the fluorescence intensity matrix may not be valid, the corresponding particles are excluded from further calculations. The remaining

profiles are then translated into a radial profile and fitted with a Gaussian profile-function according to Eq. (S1). Thereby, $I_0$ represents a scaling parameter, FWHM is the full width at half maximum, and is considered here as a measure for the patch diameter, and $I_b$ corresponds to the background correction. This process is repeated for every detected particle.

$$I_{Norm}(r) = \sqrt{4\ln 2/\pi}\frac{I_0}{FWHM} * \exp\left(\frac{4\ln 2 r^2}{FWHM^2}\right) + I_b \ (S1)$$

Furthermore, an averaged particle signal is calculated and for this averaged signal, a radial profile is determined, Figure S2 (d).

The individual FHWM values are averaged and used as a fit parameter for fitting the average radial profile with another Gaussian profile-function according to Eq. (S1) above, Figure S2(e).

The results of the averaged 3D-intensity profiles for the different stamps used are summarized in Figure S3 including the corresponding fitted average radial profiles.

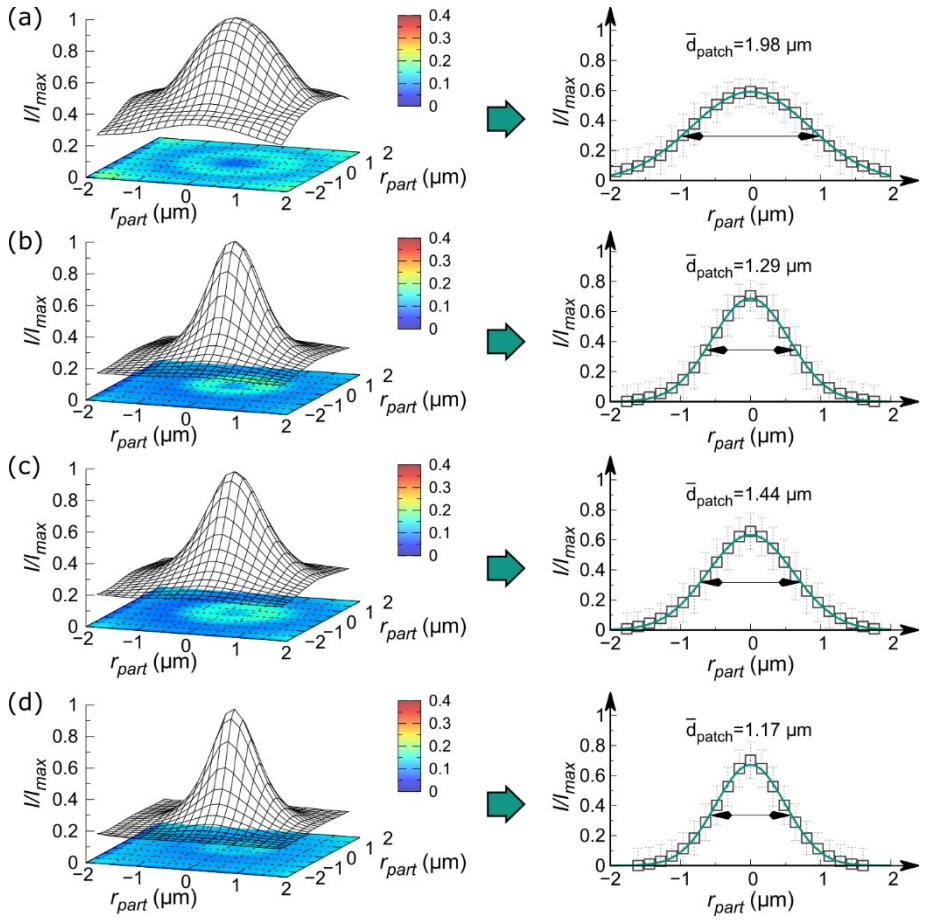


**Figure S3:** Extracted normalized fluorescence intensity profiles directly after printing averaged for >1000 particles for each stamp material used: (a) native PDMS, (b) mPEG-functionalized, (c) PNIPAAm-functionalized inked at RT, (d) PNIPAAm-functionalized inked at 45 °C. the extracted 3D profiles are converted, yielding their respective radial profiles, which is baseline corrected and fitted with a Gaussian profile function as indicated by the green curves within the plots on the right hand side. The color maps in the surface plots within the respective xy-plane represent standard deviation values originating from calculations yielding the average profile out of each individual particle profile.

It might be noted here that non-readable intensity profiles almost inclusively can be attributed to experimental phenomena. Typically, these are either when particles are not sufficiently patched with the ink, *i.e.* they have not been in contact, or ill-defined coverage is the reason resulting from local particle poly-layers that cannot be evenly printed by the stamp. Therefore, the percentage of detected but excluded particles directly reflects the printing quality in terms of yield with respect to the statistical sample being evaluated. Accordingly, this quality can be interpreted as rather high with an exclusion percentage of below 20 % (see Table S2).

## Patch profile for different printing pressures

In a typical experiment, we used PDMS-stamps, which were cut out of a PDMS mat using a circularly shaped punching device. The resulting cylindrical PDMS stamps exhibited a height of about 2 mm and radius of 0.5 cm. In order to investigate the patch profiles under varying printing pressures, we employed a 50 g and a 100 g weight on the stamps during the printing process and analysed the corresponding patch profiles directly after printing. It needs to be mentioned here that merely the printing results with a weight of 50 g have been discussed in the main article. The printing pressure is therefore estimated as follows (Eq. S2):

$$P_{print} = \frac{m_{weight}\, g}{\pi r_{stamp}^{2}} (S2)$$

Table S2 shows the patch parameters in dependence of the applied printing pressures, *i.e.* 6.25 and 12.5 kPa.

**Table S2**: Determined patch diameters from patch intensity profiles via full width at half maximum (FWHM) values after printing at two different printing pressures $P_{print}$ for the different utilized stamp types. It can be deduced that the patch diameters strongly depend on printing pressure for the case of PDMS and mPEG stamps, wherein PNIPAAm shows a comparable performance.

| Stamp type | $T_{ink}$ [°C] | $P_{print}$ [kPa] | $d_{patch}$ [µm] | Images evaluated | Particles detected | Particles evaluated | Particles excluded [%] |
|---|---|---|---|---|---|---|---|
| **PDMS** | 20-22 | 6.25 | 1.98 ± 0.51 (25.8 %) | 5 | 2696 | 2519 | 6.6 |
| | 20-22 | 12.5 | 2.00 ± 0.41 (20.5 %) | 2 | 1943 | 1828 | 5.9 |
| **mPEG** | 20-22 | 6.25 | 1.29 ± 0.30 (23.3 %) | 6 | 4993 | 4358 | 12.7 |
| | 20-22 | 12.5 | 2.17 ± 0.58 (26.8 %) | 2 | 1195 | 1058 | 11.5 |
| **PNIPAAm** | 20-22 | 6.25 | 1.44 ± 0.36 (25.0 %) | 5 | 4145 | 3625 | 12.5 |
| | 20-22 | 12.5 | 1.74 ± 0.42 (24.2 %) | 2 | 996 | 903 | 9.3 |
| | 45 | 6.25 | 1.17 ± 0.25 (21.4 %) | 5 | 2730 | 2243 | 17.8 |
| | 45 | 12.5 | 1.56 ± 0.47 (30.2 %) | 7 | 5069 | 4154 | 18.1 |

Table S2 reveals that for bare PDMS, patches of approx. 2 µm diameters are formed for both applied pressures. It can be concluded that despite the elasticity of the stamp, the pressure in the investigated range does not possess a notable influence on the printing performance. This behaviour is different for stamps which have previously been decorated with polymers, so that – in the range of pressures investigated during this study – a printing pressure dependence is merely attributed to the influence of the polymer at the stamp.

For mPEG-functionalised stamps, we observed a controllability of the patch size (to 1.29 µm) at a low pressure (6.25 kPa), whereas a doubling of the pressure resulted in the formation of patches with approximately 2.17 µm, *i.e.* a performance not better than pure PDMS, which is quite remarkable. We explain this observation by the fact that the PEG polymer network is not able to withstand the high pressure, whereupon the ink material is squeezed out of the polymer matrix. Therefore, the effect of mPEG vanishes at high pressure.

On the contrary, we did not observe this behaviour for PNIPAAm-functionalised stamps, which we explain by the capability of this polymer to form hydrogels. Due to its gel-forming nature, PNIPAAm can also sustain more printing pressure, which is well observable by the different printing results as summarised in Table S2 (1.44 µm corr. to 6.25 kPa and 1.74 µm corr. to 12.5 kPa, respectively, *vs.* 2.00 µm for bare PDMS). This effect is furthermore observable for the patchy particles printed with PNIPAAm stamps at 45 °C. These first investigations may be content for potential future work increasing the patch accuracy even further with a precisely adjusted interplay of molecular weight of the PDMS surface functionalizing polymer and printing pressure.

## Mass spectrometry data of used polymer precursor silanes

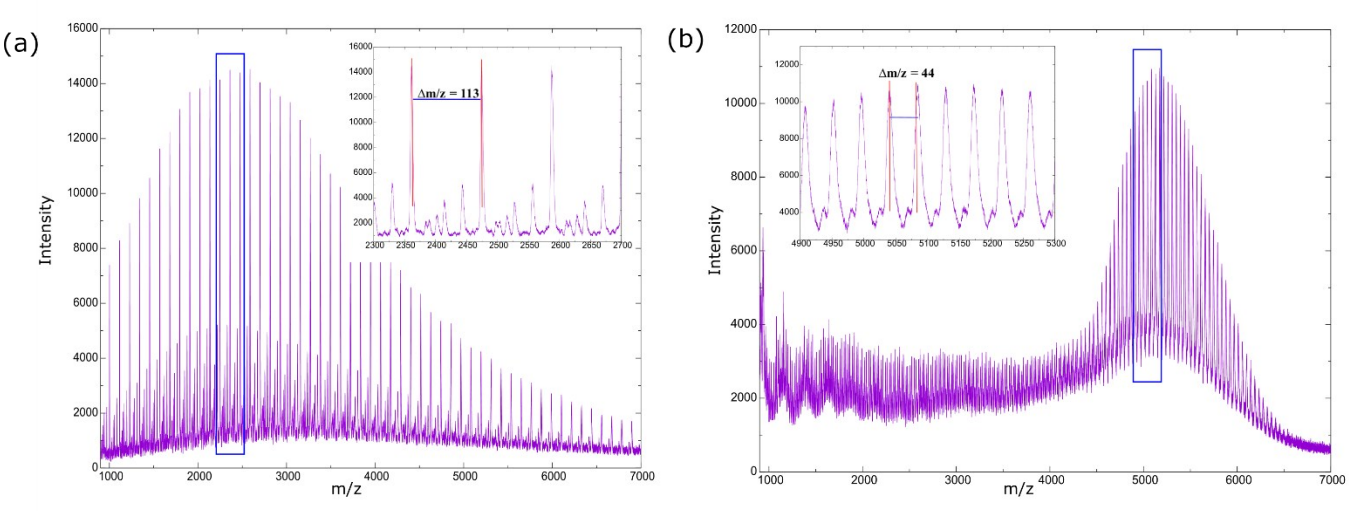


**Figure S4:** MALDI-ToF-MS spectra of the employed silane-functionalised polymers: (a) Poly(*N*-isopropylamino acrylamide) (PNIPAAm) and (b) Poly(ethylene glycol) (mPEG). The insets show a zoom-in view into their corresponding MALDI spectra as indicated by the blue boxes. The differences in molar weight of the signals highlighted with the red lines in the insets of the spectra correspond to the repeating units of the respective repeating monomer unit. Even though the chain length of the PNIPAAm polymer utilised in all experiments (approx. 2.5 kDa) is only half of that of mPEG (approx. 5 kDa), it shows an increased printing performance. For polymers with comparable molar weights, we would expect an even more pronounced superiority of PNIPAAm.
It might be argued, that an enhanced polymer chain length would lead to an increased ink layer-thickness and, therefore, an increased patch diameter. However, the polymer chain lengths are small (< 200 nm in a stretched state) compared to the patch dimensions, so that ink-flow reduction due to viscosity enhancement is here expected to be a predominant factor. This effect is more pronounced for longer polymer chains, so that increased molar weight-polymers could reduce the patch diameters even further.

## Patch profile after heating

In our experiments, we used silica particles that were pre-functionalized with 3-(aminopropyl)triethoxy silane in order to render their surface reactive *via* amino groups. As the low molecular weight ink standard, we employed rhodamine B isothiocyanate (RITC). The reactive isothiocyanate group is readily capable of forming a covalent bond with the surface amino groups on the particles (Figure 1).

We predominantly were interested in the patch profile directly after the printing process, and hence, in the performance of the polymer functionalized stamps compared to the native PDMS. However, we were also interested in investigating the patch sizes after annealing them for 75-80 °C for about 1 h, since this time span is sufficient to dry the sample and allow the reaction to complete, for which we gave evidence to this in Figure 4 showing freely dispersed particles with clear patches. In order to verify that the printing profile of the patches also translates into the final patches, we also observed the particles after heating procedure described above and characterized the patch profiles via statistical evident automatic image processing (> 1000 particles). Similarly to the experiments described in our main article, the particles were immobilized onto a glass substrate and sintered for about 1 h at 80 °C. This ensures the particles to stay on the glass substrate after the printing process, instead of their transfer onto the sticky PDMS-stamp. Table S3 summarizes the results for the different stamps directly after printing and after annealing.

**Table S3:** Determined patch diameters from patch intensity profiles *via* full width at half maximum (FWHM) values after printing and annealing at 75-80 °C for 1 h for the different utilized stamp types. It can be deduced that the patch diameters roughly stay within similar size-range while their distribution broadens by about approx. 5 %. For PNIPAAm stamps with inking temperature $T_{ink}$ at 45 °C, patch profiles after annealing were not investigated, but it is reasonable to assume a similar behaviour.

| Stamp type | | $T_{ink}$ [°C] | $d_{patch}$ [µm] | Images evaluated | Particles detected | Particles evaluated | Particles excluded [%] |
|---|---|---|---|---|---|---|---|
| **PDMS** | print | 20-22 | 1.98 ± 0.51 (25.8 %) | 5 | 2696 | 2519 | 6.6 |
| | anneal | 20-22 | 2.35 ± 0.70 (29.8 %) | 5 | 2357 | 1493 | 36.6 |
| **mPEG** | print | 20-22 | 1.29 ± 0.30 (23.3 %) | 6 | 4993 | 4358 | 12.7 |
| | anneal | 20-22 | 1.55 ± 0.44 (28.4 %) | 5 | 4284 | 3634 | 15.2 |
| **PNIPAAm** | print | 20-22 | 1.44 ± 0.36 (25.0 %) | 5 | 4145 | 3625 | 12.5 |
| | anneal | 20-22 | 1.39 ± 0.42 (30.2 %) | 5 | 3075 | 2519 | 18.1 |
| | print | 45 | 1.17 ± 0.25 (21.4 %) | 5 | 2730 | 2243 | 17.8 |
| | anneal | 45 | - | - | - | - | - |

Figure S5 shows the results for samples printed with of (a) native PDMS, (b) mPEG-functionalized, and (c) PNIPAAm-functionalized stamps, wherein the inking routine was performed at room temperature prior to the heating process.

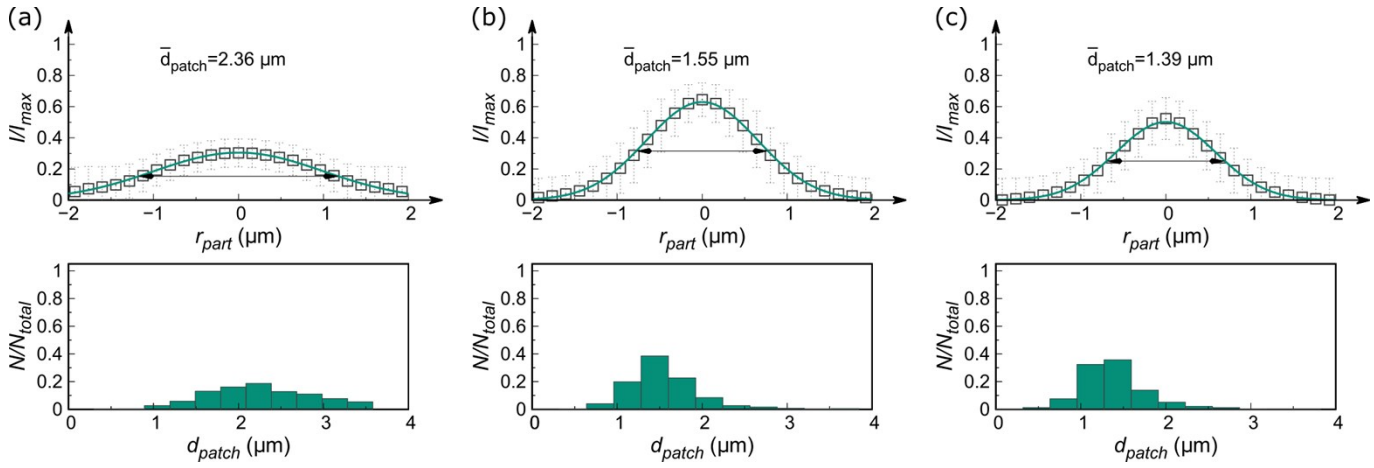


**Figure S5**: Patch profiles for particles printed and subjected to a heating process at 75-80 °C for 1 h; stamps: (a) native PDMS, (b) mPEG-functionalized, (c) PNIPAAm-functionalized; also after annealing, patch profiles are significantly sharper for the polymer grafted stamps and the trend from directly after printing is maintained. However, the patch diameter distribution is slightly broader, which may be attributed to minor ink-flow until total drying.

## References


1 S. Kim, H.-D. Choi, I.-D. Kim, J.-C. Lee, B. K. Rhee, J. A. Lim and J.-M. Hong, *J. Colloid Interface Sci.*, 2012, **368**, 9–13.

2 *ImageJ: v. 1.52h w. Java 1.8.0_172 (64-bit) available at http://imagej.nih.gov/ij*.

3 *Python packages utilised during this study: (a) Python 3.7.0 (64-bit) available at https://www.python.org; (b) Numpy: v. 1.14.5 available at https://www.numpy.org; (c) SciPy : v. 1.1.0 available at https://www.scipy.org; (d) openCV-python: v. 3.4.2 available at http://opencv.willowgarage.com/; (e) Matplotlib: v. 2.2.2 available at htts://matplotlib.org.*